

A Comparative Study of Structure–Property Relationships in Highly Oriented Thermoplastic and Thermotropic Polyesters with Different Chemical Structures

Ismail Karacan

Department of Textile Engineering, Faculty of Engineering, Erciyes University, TR-38039 Kayseri, Turkey

Received 25 April 2005; accepted 17 June 2005

DOI 10.1002/app.22554

Published online in Wiley InterScience (www.interscience.wiley.com).

ABSTRACT: Structure and properties of commercially available fully oriented thermoplastic and thermotropic polyester fibers have been investigated using optical birefringence, infrared spectroscopy, wide-angle X-ray diffraction and tensile testing methods. The effect of the replacement of *p*-phenylene ring in poly(ethylene terephthalate) (PET) with stiffer and bulkier naphthalene ring in Poly(ethylene 2,6-naphthalate) (PEN) structure to result in an enhanced birefringence and tensile modulus values is shown. There exists a similar case with the replacement of linear flexible ethylene units in PET and PEN fibers with fully aromatic rigid rings in thermotropic polyesters. Infrared spectroscopy is used in the determination of crystallinity values through the estimation of trans conformer contents in the crystalline phase. The analysis of results obtained from infrared spectroscopy data of highly oriented PET and PEN fibers suggests that trans conformers in the crystalline phase are more highly oriented than gauche conformers in the amorphous phase. Analysis of X-ray diffraction traces and

infrared spectra shows the presence of polymorphic structure consisting of α - and β -phase structures in the fully oriented PEN fiber. The results suggest that the trans conformers in the β -phase is more highly oriented than the α -phase. X-ray analysis of Vectran[®] MK fiber suggests a lateral organization arising from high temperature modification of poly(*p*-oxybenzoate) structure, whereas the structure of Vectran[®] HS fiber contains regions adopting lateral chain packing similar to the room temperature modification of poly(*p*-oxybenzoate). Both fibers are shown by X-ray diffraction and infrared analyses to consist of predominantly oriented noncrystalline (63–64%) structure together with smaller proportion of oriented crystalline (22–24%) and un-oriented noncrystalline (12–15%) structures. © 2006 Wiley Periodicals, Inc. *J Appl Polym Sci* 100: 142–160, 2006

Key words: poly(ethylene terephthalate); poly(ethylene 2,6-naphthalate); thermotropic polyesters; crystallinity; orientation

INTRODUCTION

Thermoplastic polyesters

There is considerable scientific interest in the family of thermoplastic and thermotropic polyesters produced from various combinations of aromatic rings and linear flexible chain polymers mainly due to their ease of processing, commercial success, good mechanical, chemical, and physical properties, resulting in a broad range of applications.

Poly(ethylene terephthalate) (see Fig. 1 for the chemical structure) has been one of the first commercially successful member of the family of the thermoplastic fibers.¹ Indeed, since its first commercial introduction in the late 1940s, polyester fiber found many useful roles in textile and industrial applications. In textile applications,² polyester yarns are either blended with natural fibers or texturized to give the characteristics of natural staple fibers. Heavier polyes-

ter yarns are used in industrial applications, including the automotive industry. Poly(ethylene terephthalate) (PET) is also used in the form of films and beverage bottles. Consequently, the structure and properties of polyester has been characterized using PET fibers^{3–9} and films^{10–15} using infrared^{4,6,10,12,13} spectroscopy and X-ray diffraction^{3,12,16} techniques. Suzuki and Okano⁹ prepared micro-PET fibers using CO₂ laser heating route. They produced micro-PET fibers with a birefringence of 0.234, a tensile modulus of 17.9 GPa and a tensile strength of 1.1 GPa. Middleton et al.¹² monitored the development of orientation and crystallinity of uniaxially drawn PET films in real time experiments using dynamic IR spectroscopy and X-ray diffraction measurements. Zhang et al.^{14,15} working on the ultra-thin PET films showed the variation of crystallinity with variations in film thickness values during isothermal crystallization. They attributed the reduction in crystallinity with decreasing film thickness to slower crystallization kinetics taking place during the crystallization stages. Orientation measurements also showed significant thickness dependence.

Poly(ethylene 2,6-naphthalate) (PEN), on the other hand, is a relatively new member of the commercially

Correspondence to: I. Karacan (ismaillkaracan@erciyes.edu.tr).

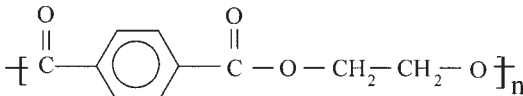
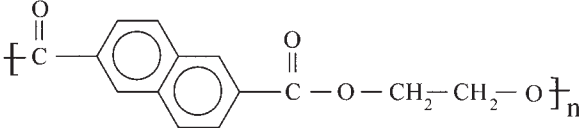
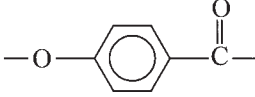
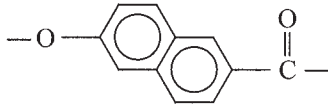
<u>FIBRE</u>	<u>STRUCTURE</u>
PET	
PEN	
VECTRAN [®] (HBA/HNA)	 HBA  HNA

Figure 1 Chemical structures of thermoplastic and thermotropic polyesters.

available thermoplastic polyesters. As shown in Figure 1, chemical structure of poly(ethylene 2,6-naphthalate) can be described by replacing the *p*-phenylene ring in PET with a stiffer naphthalene ring. Indeed, PEN is regarded as one of the high performance thermoplastic polymers because of its high thermal stability, low thermal shrinkage at elevated temperatures, high chemical and flame resistance, and good mechanical properties.

PEN fibers and films are produced commercially in Europe, North America, and Japan by well-established companies. It has already been established that such fibers and films can be obtained by conventional melt processing followed by drawing and annealing procedures. As a result, majority of work concerned with the structural characterization of PEN has been carried out using fibers,¹⁷⁻²³ films,²⁴ and melt-blended fibers with PET.²⁵ Carr et al.¹⁷ produced melt-spun PEN monofilaments about 0.5 mm thick with high strength and uniformity. Mechanical properties of these monofilaments showed a tensile modulus of 22 GPa and a tensile strength of 0.6 GPa via a single stage drawing to a draw ratio of

6.6. Cakmak and Kim¹⁹ produced fine filaments of PEN showing amorphous behavior up to processing speeds of 2500 m/min and subsequent processing speed increases, leading to semicrystalline structure containing α -form crystalline structure. They showed that processing speeds above 3500 m/min led to polymorphic structure consisting of α - and β -phase structures. Wu et al.²¹ produced fine filaments of PEN with processing speeds up to 10,000 m/min. They showed that the fiber samples developed a very high crystallinity and orientation values above processing speeds of 1500 m/min. Application of high-tension annealing to zone-annealed PEN filaments²² led to enhanced mechanical properties (tensile modulus of 33 GPa and a tensile strength of 1.1 GPa), a very high birefringence value of 0.492, and a degree of crystallinity of 57%. Realizing the importance of low thermal shrinkage and relatively good tensile properties at elevated temperatures for the production of tire cord applications, Chae et al.²³ devised a multi-step zone annealing spinning system for the production of PEN filaments.

TABLE I
Sample Details

Sample	Linear density (tex/filament)	Diameter (μm)	$n_{//}$ at 589.3 nm	n_{\perp} at 589.3 nm	Δn at 589.3 nm	IR crystallinity χ_c (%)	X-ray crystallinity χ_c (%)
PET-FOY	0.444	22.4 \pm 0.5	1.728	1.536	0.192	75%	81 %
PEN-FOY	0.447	22.5 \pm 0.5	1.895	1.560	0.335	54%- α phase 19%- β phase	83%- α phase 6%- β phase
VECTRAN [®] MK	0.555	22.5 \pm 0.5	1.965	1.570	0.395	85%	85% total order 22% crystalline 63% oriented noncrystalline
VECTRAN [®] HS	0.555	22.4 \pm 0.5	1.970	1.572	0.398	87%	88% total order 24% crystalline 64% oriented noncrystalline

High performance fibers based on liquid crystalline thermotropic polyesters

The organic conventional fibers based on linear flexible chain polymers, such as polyethylene, PET, and aliphatic polyamides, have so far proved to be inadequate for many military and industrial applications where high performance is a primary requirement.

One of the approaches to the production of high performance materials has been in the direction of the utilization of rigid chain polymers. As predicted by Flory,²⁶ rigid-rod molecules form liquid-crystals in solution forming lyotropic polymers or in the melt forming thermotropic polymers. The ability of liquid crystal structures to undergo shear orientation has enabled the production of very highly oriented filaments during spinning by the shear applied at the spinneret. As expected, such filaments exhibit outstanding tensile properties. A large number of thermotropic polymers have been synthesized and characterized. This subject has been reviewed by Dobb and McIntyre.²⁷ It has been firmly established that fibers melt spun from a nematic mesophase tend to have a very high orientation even when low winding speeds are used. Long heat-treatment of these 'as spun' fibers results in a very substantial increase of tenacity and a significant increase of extension at break.

Several thermotropic polyesters are already in production, mainly for specialist moldings with 'self-reinforcing' properties.²⁸ They are potentially useful materials for the manufacture of fibers, and indeed, Celanese Acetate LLC of USA (formerly Hoechst-Celanese) is now commercially producing Vectran[®] fibers prepared from 73% *p*-hydroxybenzoic acid (HBA) and 27% 2-hydroxy-6-naphthoic acid (HNA) units, shown in Figure 1. It is obvious that the disruption of the structure that is needed to reduce the melting temperature also hinders the crystallization. It has been found that oriented random copolymers can give a meridional X-ray diffraction pattern with well

defined but aperiodic peaks.^{29–31} Kaito et al.³² showed the variation of molecular orientation of HBA/HNA melt-extruded strands consisting of 73% HBA and 27% HNA units. They showed that the orientation was lower in the central region than in the surface region of the strands. In a similar study, Taylor et al.,³³ working on the annealed HBA/HNA fibers with the same composition, showed that the highest degree of orientation was $\sim 1 \mu\text{m}$ from the surface region of the 18 μm diameter fiber.

The aim of the present study is to characterize and compare the structure and properties of commercially available fully oriented thermoplastic polyester fibers and highly oriented liquid crystalline thermotropic copolyester fibers consisting of 73% HBA and 27% HNA units, using various methods, with the aim of establishing structure–property relationships.

EXPERIMENTAL

Materials

Fully oriented PET and PEN fiber samples were provided by Teijin Ltd of Japan and Vectran[®] fiber samples were provided by Celanese Acetate LLC of USA. All the samples were conditioned at (20 \pm 2) $^{\circ}\text{C}$ and (65 \pm 5)% RH prior the experiments. Totally four samples were studied in the present study. Details of the samples showing the linear density, diameter, refractive indices, birefringence etc. are listed in Table I.

Refractive index measurements

The refractive indices of the fiber samples with the aim of determining birefringence values were measured using an image splitting Carl Zeiss Jena interphako interference microscope. The measurements of refractive indices were carried out for wavelengths of 486.1, 551, 589.3, and 656.3 nm, respectively. The refractive

indices in the fiber axis direction ($n_{//}$) and transverse direction (n_{\perp}) were measured by matching the refractive index of Cargille immersion liquids. The measured values of the refractive indices and the birefringences for a wavelength of 589.3 nm are shown in Table I.

X-ray diffraction

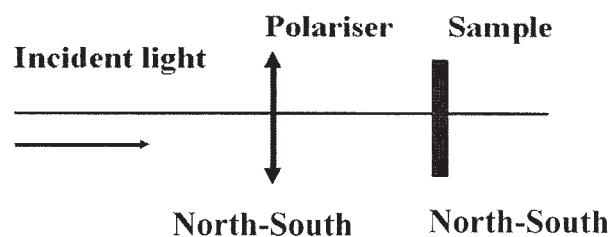
Wide-angle X-ray diffraction patterns were recorded on a flat plate at a sample to camera distance of 5 cm. The wide-angle X-ray traces were obtained using Phillips X-ray diffractometer system utilizing nickel filtered Cu K_{α} radiation (wavelength of 0.1542 nm) and voltage and current settings of 10 kV and 30 mA, respectively. Counting was carried out at 20 steps per degree. The observed equatorial and meridional X-ray scattering data was corrected for Lorentz, polarization, and incoherent scatter effects and finally normalized to a convenient standard area. Intensity corrected and normalized X-ray data were analyzed by the peak fitting procedure detailed earlier.³⁴ The peak widths at half-height have been corrected using the Stokes' deconvolution procedure.³⁵ Finally, the apparent crystallite size of a given reflection was evaluated using the Scherrer equation:

$$L(hkl) = \frac{K\lambda}{\beta \cos(\theta)} \quad (1)$$

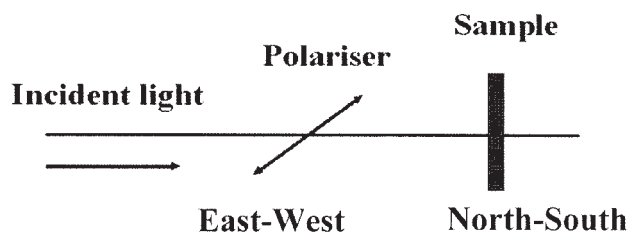
where θ is the Bragg angle for the reflection concerned, λ is the wavelength of radiation (0.1542 nm), $L(hkl)$ is the mean length of the crystallite perpendicular to the planes (hkl), β is either the integral breadth or the breadth at half maximum intensity in radians, and K is a Scherrer parameter.

Infra-red measurements

An IR-Plan® microscope installed on a Nicolet Magna IR 750 Fourier Transform spectrophotometer equipped with a ZnSe based wire grid polarizer was employed for infrared dichroic measurements. As shown in Figure 2, the fiber sample remained in a fixed North-South direction on the rotating sample stage through the experiments with the aim of using the same area in the two polarization directions and the polarizer was rotated to obtain spectra for different polarization directions. In all cases, 20 interferograms of a sample were averaged and transformed with Happ-Genzel apodization function. All the spectra were collected at a resolution of 2 cm^{-1} . Finally, all the spectra were analyzed by curve fitting procedures³⁴ to obtain accurate peak parameters.



PARALLEL POLARISATION



PERPENDICULAR POLARISATION

Figure 2 Polarized infrared sampling geometries showing the relative position of polarizer and the sample.

Tensile testing

Tensile testing measurements were carried out using Uster Tensorapid testing machine. The measurements for fully oriented PET and PEN and Vectran® MK and HS were carried out at three different gauge lengths (160, 200, and 500 mm) and at three different elongation speeds (160, 200, and 500 mm/min). For each sample, at least 20 tests were carried out to maintain the reproducibility of the results.

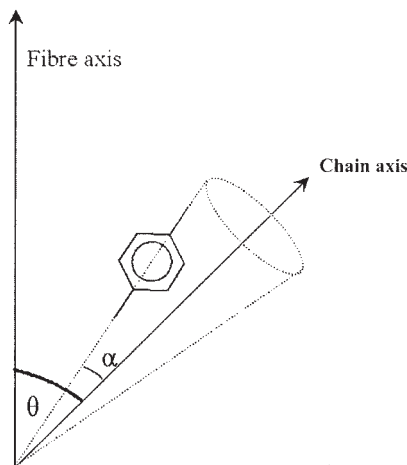
ANALYSIS OF EXPERIMENTAL DATA

Curve fitting of infrared data

The polarized infrared spectra of PET, poly(ethylene naphthalate), and Vectran fiber samples were curve fitted with a combination of Lorentzian and Gaussian profiles, according to the procedure described previously.³⁴ During the IR data collection, an average of 10 single filaments were tested to maintain the reproducibility of the results.

Calculation of orientation parameters of polarized infrared data³⁶

Because of the uniaxial orientation nature of fibers arising from cylindrical symmetry, the calculation of orientation parameters obtained from the infrared data analysis can be carried out using the dichroic ratio defined in eq. (2).



$\alpha =$ Transition moment angle
 $0 < \alpha < 90$

Figure 3 Definition of transition moment angle (α).

$$D = A_{//} / A_{\perp} \quad (2)$$

where $A_{//}$ and A_{\perp} are the measured absorbance values for radiation polarized parallel and perpendicular to the fiber axis, respectively. To a good approximation, the dichroic ratio is related to the orientation parameter $\langle P_2(\cos \theta) \rangle$ by

$$\langle P_{200} \rangle = \langle P_2(\cos \theta) \rangle = \frac{D - 1}{D + 2} \frac{2}{(3 \cos^2 \alpha - 1)} \quad (3)$$

where θ is the angle between the local chain axis and the fiber axis, and α is the transition moment angle between the associated vibrational mode and the chain axis (Fig. 3).

Calculation of crystallinity through the estimation of trans conformer content

Certain infrared bands tend to show absorbance increases following either orientation through drawing processes or during annealing stages. Usually the IR bands associated with trans conformers in crystalline phase tend to show such absorbance increases. Therefore, it has been common practice to use the absorbance or the integrated absorbance values in the evaluation of the proportion of crystalline material through the evaluation of trans conformer contents.

The total trans conformer content and hence crystalline fraction in the crystalline phase is calculated using eq. (4).¹²

$$\chi_{\text{trans}} = \frac{\sum A_{0,\text{trans}}}{\sum A_{0,\text{trans}} + \sum A_{0,\text{gauche}}} \quad (4)$$

where $\sum A_{0,\text{trans}} = A_{//\text{trans}} + 2A_{\perp\text{trans}}$ and $\sum A_{0,\text{gauche}} = A_{//\text{gauche}} + 2A_{\perp\text{gauche}}$, respectively. In the case of cis conformers, in the eq. (4), $\sum A_{0,\text{gauche}}$ will be replaced by $\sum A_{0,\text{cis}} = A_{//\text{cis}} + 2A_{\perp\text{cis}}$. $A_{//\text{trans}}$ and $A_{\perp\text{trans}}$ are the integrated absorbance values of trans bands showing parallel and perpendicular polarization characteristics and so on. Since the sum of the trans conformer content and gauche conformer content must be equal to unity, the gauche conformer content is evaluated by eq. (5).

$$\chi_{\text{gauche}} = 1 - \chi_{\text{trans}} \quad (5)$$

Calculation of crystallinity from X-ray diffraction data

X-ray crystallinity³⁷ defined as the peak area crystallinity, is based on the ratio of the integrated areas of the crystalline peaks following the peak resolution to the integrated area of the total scatter under the experimental trace. This definition can be expressed as in eq. (6)

$$\chi_c = \frac{\int_0^{\infty} I_{\text{cr}}(2\theta)d(2\theta)}{\int_0^{\infty} I_{\text{tot}}(2\theta)d(2\theta)} \quad (6)$$

The area under the background is considered to correspond to the unoriented noncrystalline scatter. In this work, the peak area crystallinity, $\% \chi_{\text{cr}}$, was estimated in the 2θ range between 10° and 35° from the peak fitting of equatorial traces.

RESULTS AND DISCUSSION

Fully oriented PET and PEN fibers

In the textile industry, melt-spun thermoplastic yarns (i.e., PET, PA6, PA6,6, and PEN, etc.) are classified according to the degree of molecular alignment introduced through different operating speeds during the fiber formation. For example, fully oriented yarn (FOY) is produced with processing speeds above 6000 m/min. The intention behind the use of increasing operating speeds is to produce continuous filament yarns with enhanced mechanical properties through increased degree of orientation along the fiber axis direction.

Analysis of optical microscopy data

Optical anisotropy is one of the most important characteristics of oriented materials and is considered to provide an overall orientation of the structural units.

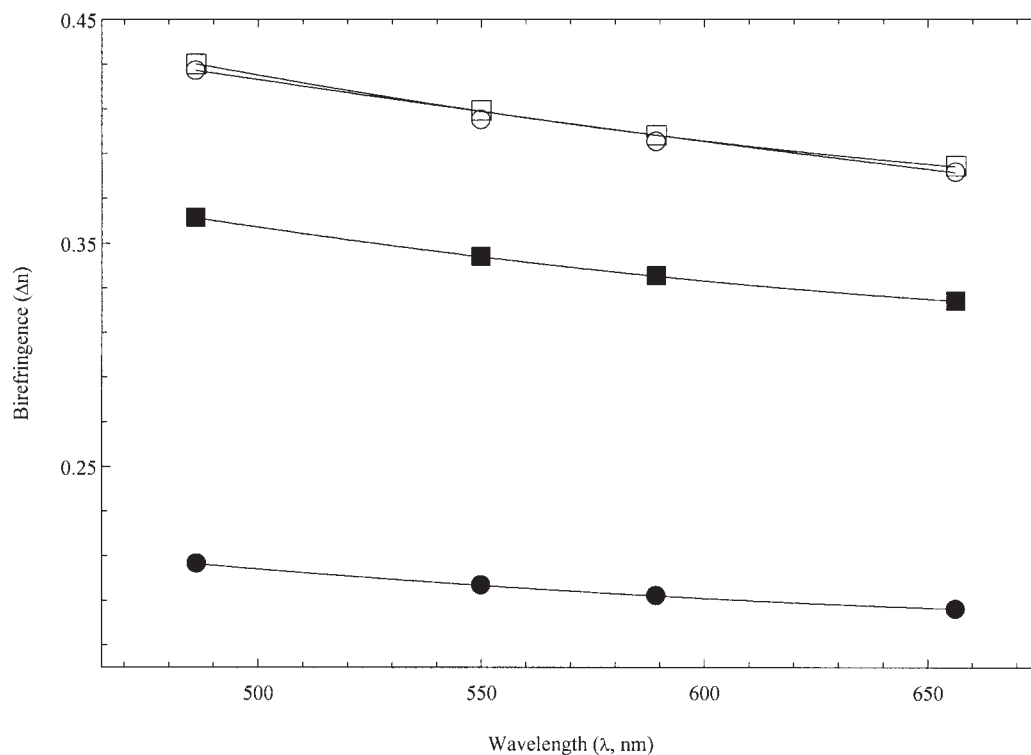


Figure 4 Variation of birefringence of polyester fiber samples with the wavelength of light used ●, fully oriented PET; ■, fully oriented PEN; ○ Vectran MK; and □, Vectran HS.

As shown in Figure 4, the birefringence values are found to decrease with increasing wavelength. This behavior is known because of the spectral dispersion. The birefringence values of fully oriented PET and PEN fibers measured at the wavelength of 589.3 nm are found to be 0.192 and 0.335, respectively, (see Table I). The high birefringence value of fully oriented PEN is believed to be due to the presence of bulky naphthalene ring.

Wide angle X-ray diffraction analysis

Fully oriented PET fiber

Crystal structure of oriented PET fiber is reported³ to be triclinic, with unit cell dimensions of $a = 0.456$ nm, $b = 0.594$ nm, and $c = 1.075$ nm, and unit cell angles of $\alpha = 98.5^\circ$, $\beta = 118^\circ$, and $\gamma = 112^\circ$. As shown in Figure 5(a), wide-angle X-ray diffraction pattern shows that fully oriented PET fibers possess very high molecular orientation as indicated by the low azimuthal arching of equatorial and off-meridional reflections together with very high degree of crystallinity characterized by the presence of well-defined and strong off-equatorial and off-meridional reflections.

The equatorial trace shown in Figure 6(a) can be resolved into at least three crystalline peaks indexed as 010, $\bar{1}10$, and 100 peaks. During the curve fitting stages, it was necessary to introduce a broad noncryst-

alline peak with a d -spacing of 0.443 nm to improve the fitting. This peak is labeled as NC and is believed to be due to the oriented noncrystalline material. The corresponding d -spacings, half-height widths, and crystallite sizes are summarized in Table II. The results

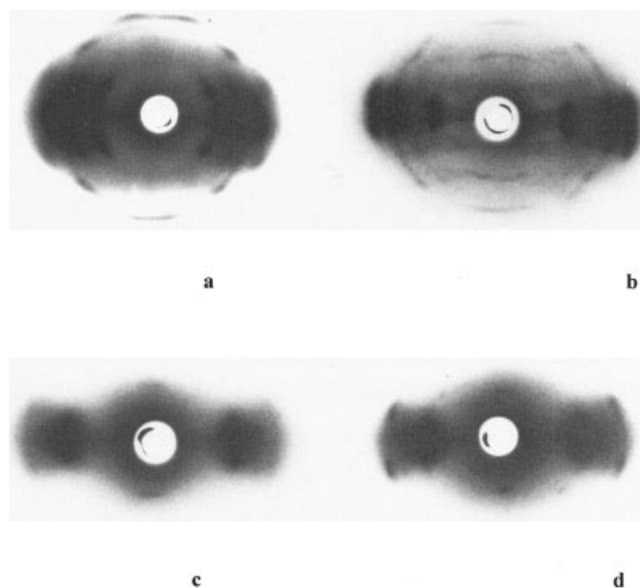


Figure 5 Wide-angle X-ray diffraction patterns of (a) fully oriented PET, (b) fully oriented PEN, (c) oriented Vectran MK, and (d) oriented Vectran HS fiber.

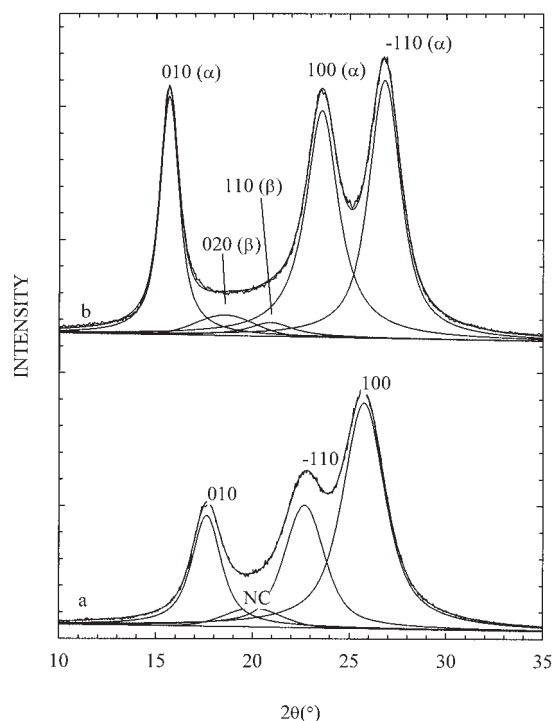


Figure 6 Curve fitting of equatorial diffraction trace of (a) fully oriented PET fiber, and (b) fully oriented PEN fiber.

suggest crystallite sizes perpendicular to the, (010), (110), and (100) planes as 4.71, 3.35, and 3.27 nm, respectively, corresponding to at least 81 laterally packed chains along the fiber axis direction. As shown in Table I, the X-ray crystallinity for this sample is found to be 81% together with 4% oriented noncrystalline material.

Fully oriented PEN fiber

Crystalline structure of PEN is reported to have two crystalline forms. α -form³⁸ is reported to have the unit

cell dimensions where $a = 0.651$ nm, $b = 0.575$ nm, and $c = 1.32$ nm and unit cell angles where $\alpha = 81.33^\circ$, $\beta = 144^\circ$, and $\gamma = 100^\circ$ with one chain per unit cell. The crystalline density of α -form is reported³⁸ to be 1.407 g/cm³. The second crystalline form (i.e., β -crystalline form)³⁹ is reported to have the unit cell dimensions where $a = 0.926$ nm, $b = 1.559$ nm, and $c = 1.273$ nm, and unit cell angles where $\alpha = 121.6^\circ$, $\beta = 95.57^\circ$, and $\gamma = 122.52^\circ$ with four chains per unit cell. In the α -form, the polymer chains are in the fully extended conformation, whereas in the β -form, the polymer chains are less fully extended.

As shown in Figure 5(b), wide-angle X-ray diffraction pattern shows that the fully oriented PEN fibers possess very high molecular orientation as indicated by the low azimuthal arching of equatorial and off-meridional reflections together with very high degree of crystallinity indicated by the presence of well defined and strong off-equatorial and off-meridional reflections.

The equatorial trace shown in Figure 6(b) can be resolved into at least three crystalline peaks indexed as 010, 100, and $1\bar{1}0$ peaks with d -spacings of 0.565, 0.377, and 0.332 nm of α -phase. During the curve fitting stages, it was necessary to introduce two broad peaks with d -spacings of 0.478 and 0.424 nm close to the d -spacings of 020 and 110 peaks of β -phase. The corresponding half-height widths and crystallite sizes are summarized in Table II. The results suggest crystallite sizes perpendicular to the, (010), (100), and (110) planes of α -phase as 7.3, 4.45, and 4.4 nm, respectively, corresponding to oriented at least 156 laterally packed chains along the fiber axis direction. As shown in Table I, X-ray crystallinity for this sample is found to be 89% consisting of 83% α -phase and 6% β -phase, respectively. Consequently, the proportion of unoriented noncrystalline (i.e., amorphous) phase is found to be 11%. It is reported by Miyata et al.¹⁸ that the proportion of α -phase relative to the proportion of

TABLE II
Calculation of Apparent Crystallite Sizes Obtained from Resolved Equatorial X-Ray Diffraction Traces of Fully Oriented PET and PEN Fibres

hkl indexing	Observed d -spacing (nm)	Experimental half-height width (2θ , deg)	Corrected half-height width (2θ , deg)	$L_{(hkl)}$ apparent crystallite size (nm)
PET-FOY				
010	0.504	1.94	1.90	4.71
$\bar{1}10$	0.392	2.74	2.69	3.35
100	0.346	2.82	2.78	3.27
$\bar{1}05$	0.211	2.31	2.27	4.18
PEN-FOY				
010(α)	0.565	1.26	1.22	7.30
020(β)	0.478	4.27	4.21	2.13
110 (β)	0.424	2.76	2.73	3.29
100(α)	0.377	2.06	2.03	4.45
$\bar{1}10(\alpha)$	0.332	2.10	2.06	4.40

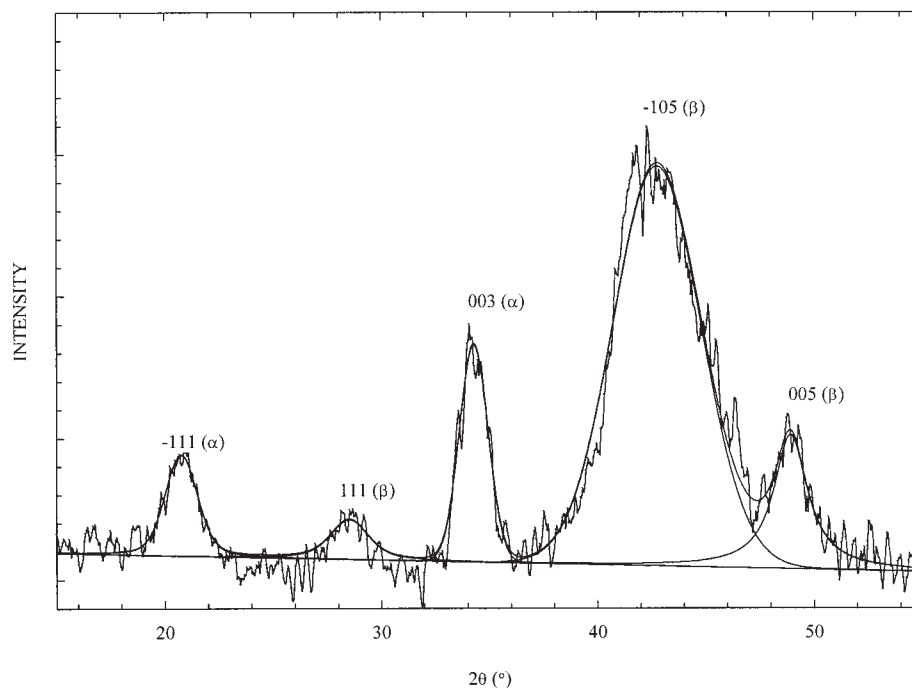


Figure 7 Curve fitting of meridional diffraction trace of fully oriented PEN fiber.

β -phase decreases with increasing processing speeds. It suggests that molecular alignment of chains due to increasing processing speeds encourages the formation of polymorphism with greater proportion of β -phase at high take-up speeds.

Figure 7 shows two genuine meridional reflections as well as two off-equatorial and one off-meridional reflections intersecting the meridional region due to the considerable azimuthal spread. In particular, the peak at 0.428 nm is the intersection of (-111) reflection of α -phase crystalline structure. The peak with a d -spacing of 0.313 nm is the intersection of (111) reflection of β -phase crystalline structure. The first genuine meridional peak with a d -spacing of 0.2615 nm is indexed as (003) reflection of α -phase. The peak with a d -spacing of 0.211 nm is the intersection of (-105) off-meridional reflection of β -phase structure. The second genuine meridional peak with a d -spacing of 0.186 nm is indexed as (005) reflection of β -phase crystalline structure. It shows that the crystalline structure of fully oriented PEN fiber is indeed polymorphic as shown by the presence of meridional reflections due to the presence of α - and β -phase structures.

Analysis of infrared spectroscopy data

Fully oriented PET fiber

It has been demonstrated that there are few bands that show changes in intensities following the heat treatments.⁴ This shows that the changes associated with the crystallinity can be followed accurately using these

specific bands. There are also bands sensitive to the conformation of the ethylene glycol units ($-\text{O}-\text{CH}_2-\text{CH}_2-\text{O}-$). The ethylene glycol units can adopt trans and gauche conformations through the internal rotation of C—C bond. The trans conformation has been shown to exist in the crystalline phase and the gauche conformation in the unoriented non-crystalline (i.e. amorphous) phase.⁴ Subsequent studies⁴ indicated that the gauche conformation can also exist in both crystalline and amorphous phase. Therefore, the crystalline and amorphous proportions can be estimated reasonably accurately by evaluating the trans and gauche conformer contents.

The parallel and perpendicular spectrum in the 1050–750 cm^{-1} region, shown in Figure 8(a), is fitted with bands based on combination of Gaussian and Lorentzian profiles [Fig. 8(b)], according to a curve fitting procedure detailed earlier.³⁴ The peak parameters in terms of peak positions and bandwidths are taken from the literature.⁴

The total trans conformer content in the crystalline phase is calculated as the sum of the integrated absorbance values of the 962, 973, and 978 cm^{-1} bands, whereas the total gauche conformer content in the unoriented noncrystalline (i.e. amorphous) phase is calculated as the sum of the integrated absorbance values of 890, 899, and 906 cm^{-1} bands. The total trans conformer content, and hence crystalline fraction in the crystalline phase, is calculated¹² according to the eq. (4).

The IR band at 962 cm^{-1} is assigned⁴ to the trans conformations of glycol units in the oriented amor-

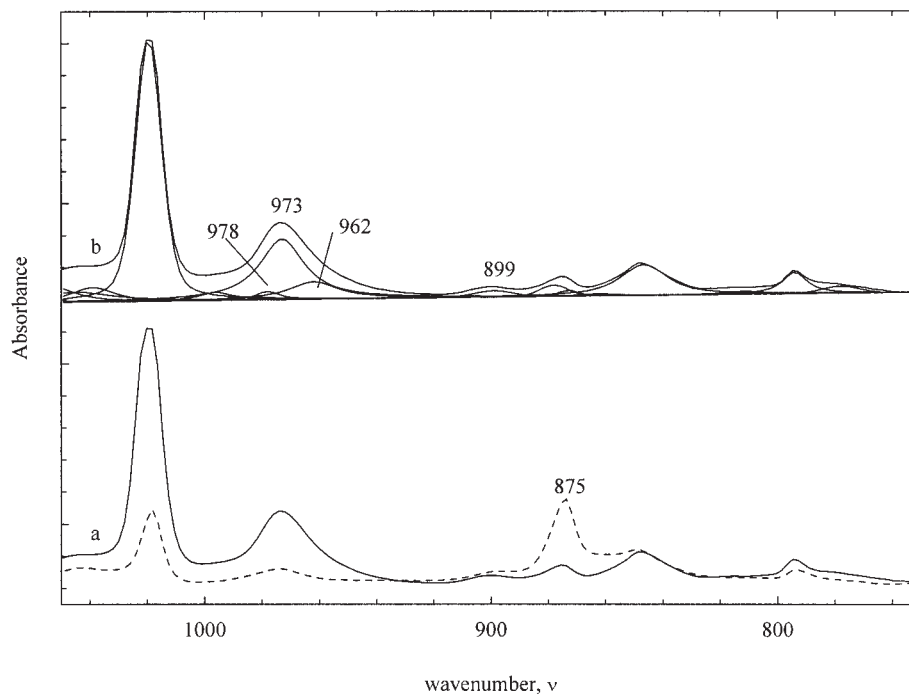


Figure 8 Polarised infrared spectrum of fully oriented PET fiber. Parallel polarization spectrum (solid line) and perpendicular polarization (broken line) (a) and an example of curve fitting (b).

phous material. In the present investigation, 973 cm^{-1} trans band has been used for the determination of the crystallinity, as suggested in the literature.⁴

Using the trans bands located at 962, 973, and 978 cm^{-1} and gauche bands located at 890, 899, and 906 cm^{-1} , via eq. (4) following the determinations of integrated absorbance values from curve fitting procedure, a trans content (and hence crystalline fraction) of 75% in the crystalline phase and a gauche content of 25% in the amorphous phase was obtained using eq. (5) (Table I).

During the calculations, 794 cm^{-1} IR band was used as an internal calibration to normalize the full spectrum because of possible thickness variations between the samples. The results in Table III show that trans conformers represented by 973 cm^{-1} vibration in the crystalline phase is slightly more oriented than the *p*-phenylene ring represented by 873 cm^{-1} IR band.

It should be noted that the transition moment angle of *p*-phenylene ring is found to be 20.9° , using the atomic coordinates given by Daubeny et al.³ In the

case of the 873 cm^{-1} band, a value of 85° is used as suggested in the literature.⁴⁰ A transition moment angle of 33° is used as suggested in the literature⁴ for the trans conformer in the crystalline phase represented by 973 cm^{-1} band. Same transition moment angle of 33° is also used for the 962 cm^{-1} assigned by Yazdani et al.⁴ to the trans conformers in the oriented amorphous phase.

Orientation parameter ($\langle P_2 \rangle$) corresponding to the trans conformers in the crystalline phase and gauche conformers in the amorphous phases are evaluated using eq. (3) and the results are listed in Table III. As expected the gauche conformers represented by 899 cm^{-1} vibration in the amorphous phase ($\langle P_2 \rangle = 0.42 \pm 0.05$) is less oriented than the trans conformers in the crystalline ($\langle P_2 \rangle = 0.89 \pm 0.05$) and oriented amorphous ($\langle P_2 \rangle = 0.65 \pm 0.05$) phases.

Fully oriented PEN fiber

The IR spectrum of PEN in the $1650\text{--}1310\text{ cm}^{-1}$ region shown in Figure 9 contains bands attributed to crystalline and amorphous phases arising from the presence of vibrations of trans and gauche conformers of CH_2 moieties and the naphthalate ring, respectively. Carbonyl ($\text{C}=\text{O}$) stretching vibration is seen at $1715\text{--}1720\text{ cm}^{-1}$, showing perpendicular polarization characteristics. Naphthalene ring vibrations are located at 1602 , 1503 , and 1406 cm^{-1} , showing parallel polarization characteristics⁴¹ [see Fig. 9(a)].

TABLE III
 $\langle P_2 \rangle$ Values of Fully Oriented PET Fibre Obtained from IR Data

Assignment	$\langle P_2 \rangle$
Benzene ring (873 cm^{-1})	0.85 ± 0.05
CH_2 gauche (899 cm^{-1})	0.42 ± 0.05
CH_2 trans (962 cm^{-1})	0.65 ± 0.05
CH_2 trans (973 cm^{-1})	0.89 ± 0.05

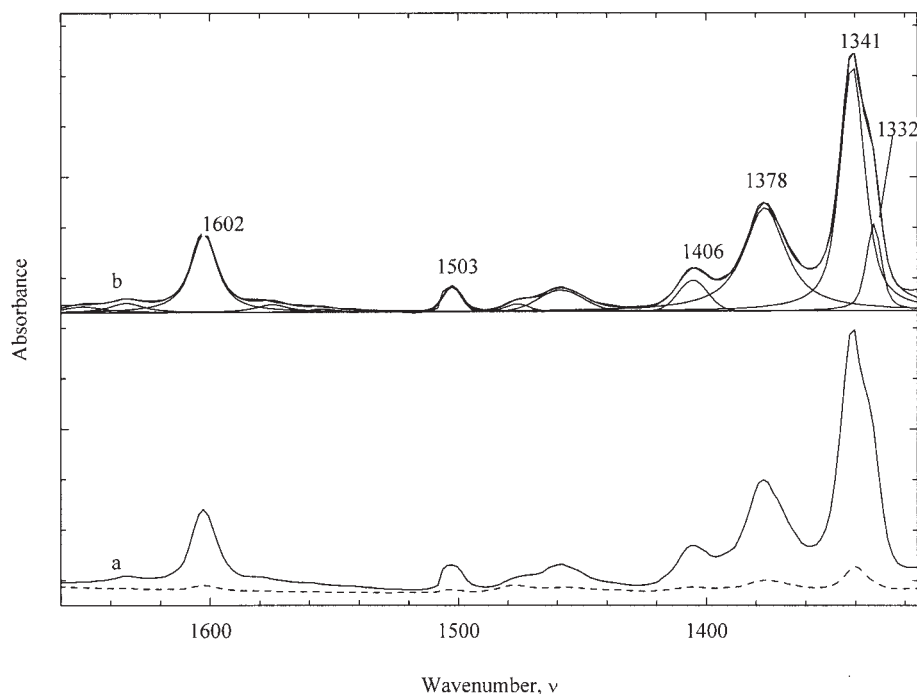


Figure 9 Polarised infrared spectrum of fully oriented PEN fiber. Parallel polarization spectrum (solid line) and perpendicular polarization (broken line) (a) and an example of curve fitting (b).

According to Ouchi et al.,⁴¹ the IR band at 1332 cm^{-1} due to the wagging mode of CH_2 conformers is found to increase after drawing and annealing and is said to be attributed to the trans conformers in the crystalline phase, and the vibration at 1377 cm^{-1} due to the wagging mode of CH_2 conformers is said to be attributed to the gauche conformers in the amorphous phase. The IR band at 1341 cm^{-1} is also attributed to the trans conformers in the crystalline phase. As mentioned above, in the highly oriented PEN fibers, the presence of polymorphism with α - and β -phases is observed in the wide-angle diffraction analysis. It is highly likely that the IR band at 1341 cm^{-1} is due to the α -phase and the new and emerging band at 1332 cm^{-1} seen as a shoulder after annealing and drawing processes is due to the β -phase. All the spectra involved in the calculations are normalized using the IR band at 767 cm^{-1} . This band is reported to have no intensity changes following drawing and annealing experiments.²⁴

Because of the over saturation of the bands and polarizer-related uncertainties in the 1850–1650 cm^{-1} (including C=O stretching vibration at 1715–1720 cm^{-1}) and 1300–1050 cm^{-1} region containing combination of naphthalene ring vibrations and ethylene glycol vibrations, no meaningful results can be obtained. Transition moment angle (α) for the naphthalene ring is evaluated as 23° using the atomic coordinates of α -phase crystalline structure of Mencik.³⁸ Transition moment angle (α) of ethylene glycol (O—C) link with the naphthalene ring is determined to be as 15° from the atomic coordinates of Mencik.³⁸

The orientation parameters listed in Table IV, as expected, show higher orientation of trans conformers in the crystalline phase than the gauche conformers in the amorphous phase. The results suggest that the trans conformers in the β -phase is more highly oriented than the α -phase. The $\langle P_2 \rangle$ value of 1341 cm^{-1} due to trans conformers in the α -phase is found to be 0.86 ± 0.02 , whereas the $\langle P_2 \rangle$ value for the 1332 cm^{-1}

TABLE IV
 $\langle P_2 \rangle$ Values of Fully Oriented PEN Fiber Obtained from IR Data

	1602 cm^{-1}	1503 cm^{-1}	1378 cm^{-1} CH_2 - wagging gauche	1344 cm^{-1} CH_2 - wagging trans- α -phase	1332 cm^{-1} CH_2 - wagging trans- β -phase
$\langle P_2 \rangle$	0.84 ± 0.04	0.75 ± 0.06	0.54 ± 0.06	0.86 ± 0.02	0.92 ± 0.04
Transition moment (α)	23°	23°	0°	15°	15°

TABLE V
Total Trans and Gauche Conformer Contents of Fully Oriented PEN Fiber

χ_{trans} due to β -phase (1332 cm^{-1})	$(19 \pm 3)\%$
χ_{trans} due to α -phase (1341 cm^{-1})	$(19 \pm 3)\%$
Total χ_{trans} $\alpha + \beta$ phase	$(73 \pm 2)\%$
Total χ_{gauche}	$(27 \pm 2)\%$

due to the trans conformers in the β -phase is found to be 0.92 ± 0.04 , assuming a transition moment angle of 15° for both vibrations. Because of the absence of published information on the exact direction of the gauche conformer in the amorphous phase, a value of 0° is used as the transition moment angle for the 1378 cm^{-1} band. The gauche conformers in the amorphous phase represented by 1378 cm^{-1} vibration is found to have an average $\langle P_2 \rangle$ value of 0.54 ± 0.06 .

In the case of the naphthalene ring vibrations, the band at 1602 cm^{-1} is found to have the highest dichroic ratio among the naphthalene ring vibrations with an average $\langle P_2 \rangle$ value of 0.84 ± 0.04 , assuming a transition moment angle of 23° . The naphthalene vibration at 1503 cm^{-1} is found to have an average $\langle P_2 \rangle$ value of 0.75 ± 0.06 .

Using eqs. (7) and (8), the α - and β -phase trans conformer contents are evaluated using the integrated absorbance values of the IR bands at 1341 cm^{-1} representing α -phase and 1332 cm^{-1} representing β -phase as trans conformers of CH_2 wagging vibration in the crystalline phase and 1378 cm^{-1} as a gauche conformer due to CH_2 wagging vibration in the amorphous phase. As shown in Table V, the total trans conformer content of 73% is found to consist of α - and β -phases. The results suggest trans conformer contents in the α - and β -phases of $(54 \pm 2)\%$ and $(19 \pm 3)\%$, respectively. As a result, the gauche conformer content in the amorphous phase is found to be 27%. Assuming further contributions of trans conformer content in the amorphous phase, there is no doubt that the total trans conformer content is bound to be ever higher than 73%.

Mechanical properties

The measured mechanical properties of fully oriented PET fiber in terms of tensile strength, elongation at break, and tensile modulus are listed in Table IX. The results suggest a small but systematic reduction in the tensile strength and elongation at break and an increase in the tensile modulus as the cross-head speed is increased from 160 to 500 mm/min. The results suggest a tensile strength of 0.9–1.06 GPa, an elongation at break of 9.4–11.4%, and a tensile modulus of 9.7–12.3 GPa, depending on the testing conditions. The theoretical tensile modulus of PET at room temperature is reported to be 108 GPa in the literature.⁴²

The average experimental value of tensile modulus (10.77 GPa) corresponds to $\sim 10\%$ of the theoretical value. It is clear that there is still much room for the enhancement and improvement of the tensile modulus of fully oriented PET fiber.

Turning to fully oriented PEN fiber, measured mechanical properties with a constant strain rate of 100% per minute listed in Table IX suggest a tensile strength of 0.89–0.98 GPa, an elongation at break of 9.4–11.0%, and a tensile modulus of 19.9–20.6 GPa, depending on the testing conditions. The theoretical tensile modulus of PEN at room temperature is reported to be 145 GPa.⁴² The average experimental value of tensile modulus corresponds to $\sim 14\%$ of the theoretical value. It is also clear that there is still room for the enhancement and improvement of the tensile modulus of PEN fiber.

Structure and properties of thermotropic copolyester fibres

The melt spun fibers of thermotropic copolyesters prepared from 73 mol % HBA and 27 mol % HNA³³ are marketed under the trade name of Vectran by Celanese Acetate LLC (Formerly Hoechst Celanese Corp). Commercially, Vectran MK and Vectran HS variants are available. It seems that Vectran MK is the original 'as spun' fiber without any processing after the melt spinning, whereas Vectran HS is the annealed version of Vectran MK, as indicated by the wide-angle X-ray diffraction patterns. Because of commercial reasons, the annealing conditions are not released to the general public. As shown in Figures 10 and 11, approximately colinear HBA and HNA units connected through ester linkages in the backbone molecular chains lead to a stiff and extended chain conformations, which are a primary requirement for the formation of oriented mesophases in the melt to exhibit thermotropic behavior.

Analysis of optical microscopy data

As shown in Table I and Figure 4, the measured birefringence value of Vectran MK fiber shows no significant difference from that of Vectran HS fiber. It is also clear that the birefringence values are considerably high ($\Delta n = 0.395\text{--}0.398$) and indicate a very high overall orientation despite relatively low proportion of crystalline material in both fibers.

Wide-angle X-ray diffraction data

Chemical structures of the constituent units of copolyester chains are shown in Figure 1. HNA is used in the copolymerization stage to reduce the melting temperature to obtain a liquid-crystalline phase at a temperature below that of decomposition via randomization of the ester group direction.

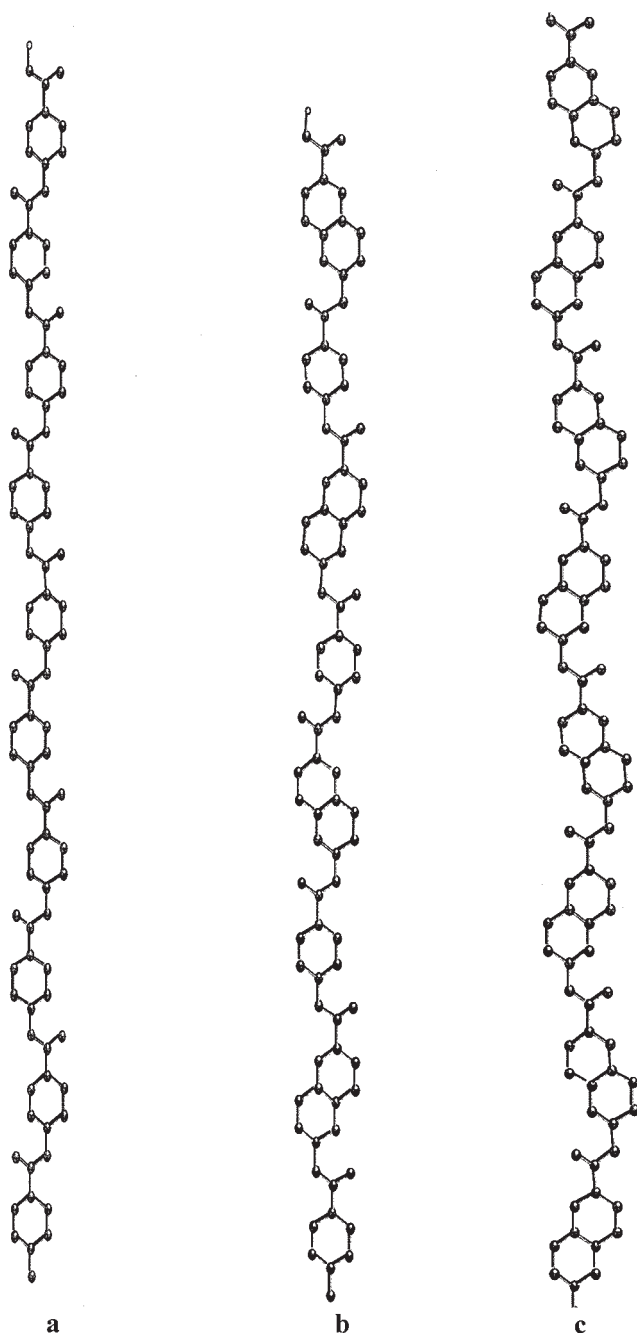


Figure 10 Regular chain sequences of (a) *cis*-poly(*p*-oxybenzoate), (b) alternating *cis-trans* HBA/HNA, and (c) *cis*-poly(*p*-penylene 2,6-naphthalate).

As shown in Figure 10(a), HBA units are contained in the structure of poly(*p*-oxybenzoate) (POB). The melting temperature of POB is found to be too high (610°C) for conventional melt processing. Because of the processing problems, POB never gained industrial importance. POB can be viewed as the 'parent homopolymer' of a large group of thermotropic copolyesters. Indeed, poly(*p*-oxybenzoate-*co*-ethylene terephthalate)⁴³ featured prominently in the development of thermotropic liquid crystalline polymers. Be-

cause of their commercial availability, these materials were widely studied.⁴⁴ Copolymers containing *p*-oxybenzoyl and 2-hydroxy-6-naphthaloyl units (75/25 to 40/60) are highly promising, and were studied in great detail.^{29-33,45-50}

Lieser⁵¹ examined poly(*p*-oxybenzoate) and its oligomers by means of both X-ray and electron diffraction techniques; evidence of polymorphism was found and it was assumed that this was a result of different conditions of crystal formation. The two different forms of crystal structures at room temperature were named as Type I and Type II. The most common crystal form observed is an orthorhombic unit cell with cell dimensions of $a = 0.752$ nm, $b = 0.570$ nm, and $c = 1.249$ nm. This unit cell contains two chains in a 2_1 helical conformation. Type II structure is also orthorhombic with unit cell dimensions of $a = 0.377$ nm, $b = 1.106$ nm, and $c = 1.289$ nm. Lieser⁵¹ showed that the crystalline structure of poly(*p*-oxybenzoate) was transformed to Type III structure at elevated structure where the prominent (110) and (200) reflections of Type I structure merged. Consequently,

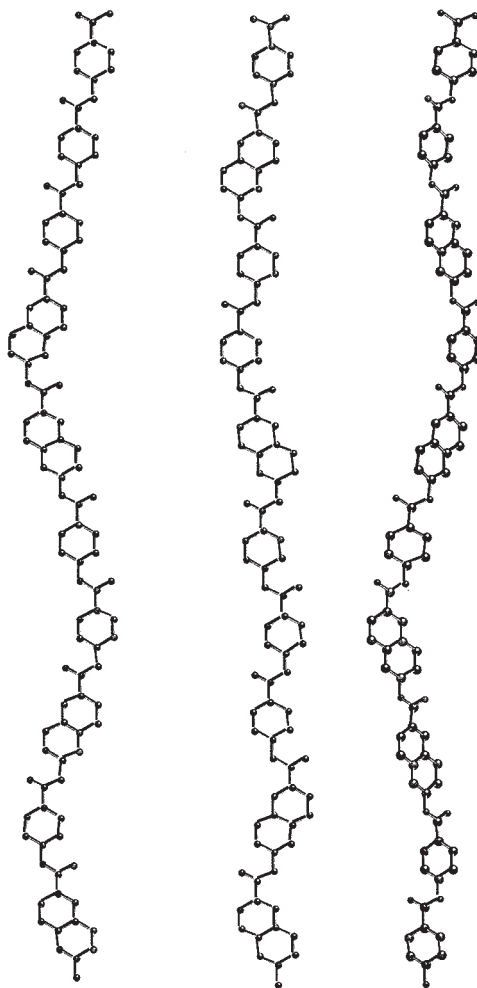


Figure 11 Random HBA/HNA copolymer chains.

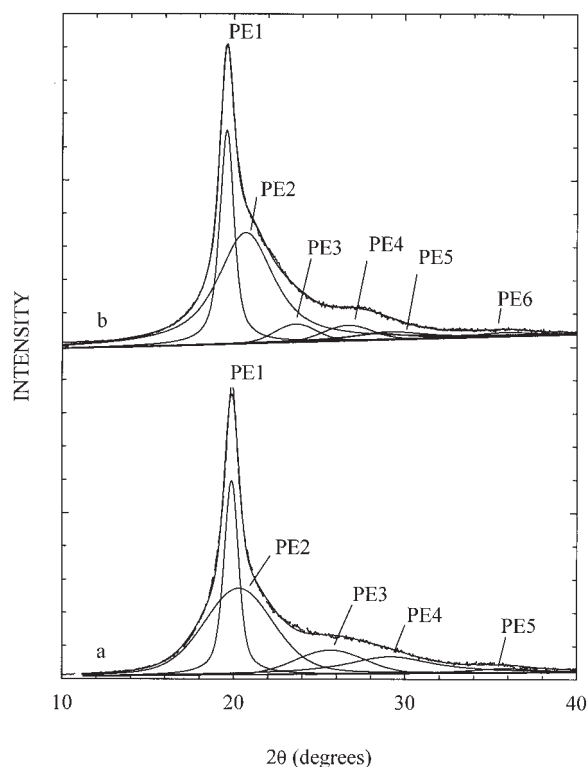


Figure 12 Curve fitting of equatorial diffraction traces of (a) Vectran MK fiber and (b) Vectran HS fiber.

Lieser⁵¹ suggested an orthorhombic unit cell where $a = 0.92$ nm, $b = 0.53$ nm, and $c = 1.24$ nm. Subsequently, Coulter et al.⁵² carried out a detailed investigation of poly(*p*-oxybenzoate) at elevated temperatures above 350°C and found a new orthorhombic

crystal structure where $a = 0.913$ nm, $b = 0.535$ nm and $c = 1.249$ nm. This unit cell is essentially very similar to Lieser's Type III structure. The d -spacing of the most prominent (110/200) reflection is around 0.46 nm.

Qualitative analysis of wide-angle X-ray diffraction patterns of Vectran MK ('as spun') fiber shown in Figure 5(c) shows a broad asymmetrical equatorial scatter centered around a d -spacing of 0.44 nm assigned to a pseudohexagonally packed oriented noncrystalline structure. The wide-angle X-ray diffraction pattern of Vectran HS fiber shown in Figure 5(d) shows the initial signs of three-dimensional order, as shown by the additional off-equatorial reflections on the nonperiodic layer lines. Quantitative analysis of Vectran MK and Vectran HS fibers are carried out utilizing equatorial and meridional scans.

Equatorial X-ray diffraction analysis of Vectran MK fiber

Resolved equatorial trace of Vectran MK fiber shown in Figure 12(a) can be resolved into at least five peaks (see Table VI for peak parameters). The first peak at 0.46 nm is close to the d -spacing of (110/200) reflection of Type III orthorhombic structure of poly(*p*-oxybenzoate).⁵¹ The second peak at 0.44 nm is broad and can be assigned to the pseudohexagonally packed oriented noncrystalline structure. The third peak at 0.347 nm is close to the (210) reflection of Type III orthorhombic structure. The fourth peak at 0.307 nm is close to the d -spacing of (300) reflection of Type III structure. Finally, the fifth peak at 0.25 nm is close to the

TABLE VI
Calculation of Apparent Crystallite Sizes Obtained from X-Ray Diffraction Traces of Vectran[®] MK and HS Fibers

Sample	Peak	Observed d -spacing (nm)	Experimental half-height width (2θ , deg)	Corrected half-height width (2θ , deg)	$L_{(hkl)}$ apparent crystallite size (nm)	
Vectran [®] MK	Equatorial peaks	PE1	0.459	1.12	1.07	8.3
		PE2	0.435	5.55	—	—
		PE3	0.347	5.67	—	—
		PE4	0.307	6.13	—	—
		PE5	0.251	4.62	—	—
	Meridional peaks	PM1	0.664	2.15	2.10	—
	PM2	0.308	4.17	4.11	—	
	PM3	0.207	2.20	2.14	—	
Vectran [®] HS	Equatorial peaks	PE1	0.454	1.07	1.02	8.8
		PE2	0.429	4.12	—	—
		PE3	0.376	3.36	3.3	—
		PE4	0.335	3.97	—	—
		PE5	0.307	4.07	—	—
		PE6	0.250	4.14	—	—
	Meridional peaks	PM1	0.666	2.00	1.96	—
		PM2	0.306	2.63	2.57	—
		PM3	0.207	2.06	2.01	—

d-spacing of (121) reflection of Type III structure intersecting the equatorial region.

The results suggest the presence of the lateral chain packing as in the high temperature modification of poly(*p*-oxybenzoate) coded as Type III structure. It appears that there is a similar situation with the 75/25 composition of as spun fiber.⁴⁵ The presence of high temperature modification of poly(*p*-oxybenzoate) is not surprising in the Vectran MK fiber because 73 mol % of HBA units make up the polymer structure together with the remaining amount of 27% of the structure consisting of HNA units. The resolved peak parameters in terms of *d*-spacings, experimental, and corrected half-height widths and the corresponding apparent crystallite sizes using the Scherrer equation are listed in Table VI. Since all the peaks are found to be very broad with high half-height widths, crystallite size is only evaluated for the peak at 0.46 nm as 6.15 nm corresponding to 13 laterally packed chains in the direction perpendicular to the (200) planes of Type III poly(*p*-oxybenzoate) structure.

As shown in Table I, the curve fitting analysis reveals that 85% of the area above baseline is due to the oriented and ordered structure. This means that the Vectran MK fiber consists of 15% unoriented noncrystalline (i.e., amorphous) structure. Assuming that the peak at 0.459 nm is close to the *d*-spacing of (200) reflection of Type III structure due to its strength and sharpness, a crystalline proportion of 22% is found. This means that we have an oriented noncrystalline content of 63%. The value of 22% crystallinity is close to the value of 21% found⁴⁶ for the unannealed 6 mm rods of 75/25 composition. Blundell⁴⁷ also found an average X-ray crystallinity value of 21% for the 40% HBA and 60% HNA composition hand drawn fibers. Crystallite size obtained from the corrected half-height width of the peak at 0.459 nm is found to be 8.3 nm. A similar dimension of 10 nm was obtained⁴⁸ using transmission electron microscopy for the Vectra® A950 thin films (thickness about 50 nm) consisting of 73% HBA and 27% HNA units. Blundell⁴⁷ reported a lateral crystallite size of 10 nm for the hand drawn HBA/HNA fiber consisting of 40% HBA and 60% HNA units.

Equatorial X-ray diffraction analysis of Vectran HS fiber

Resolved equatorial trace of Vectran HS fiber shown in Figure 12(b) can be resolved into at least 6 peaks (see Table VI for peak parameters). The first peak at 0.454 nm is close to the *d*-spacing of (110) reflection of Type I orthorhombic structure of poly(*p*-oxybenzoate).⁵¹ The second peak at 0.429 nm is broad and can be assigned to the pseudohexagonally packed oriented noncrystalline structure. The third peak at 0.376 nm is close to the (200) reflection of Type I orthorhom-

bic structure. The fourth peak at 0.347 nm is close to the *d*-spacing of (210) reflection of Type III orthorhombic structure. The fifth peak at 0.335 nm is close to the *d*-spacing of (211) reflection of Type III orthorhombic structure intersecting the equatorial region. The sixth peak at 0.307 nm is close to the *d*-spacing of (300) reflection of Type III structure. Finally, the seventh peak at 0.25 nm is close to the *d*-spacing of (300) reflection of Type I structure.

It appears that Vectran HS fiber possesses a multiphase structure consisting of oriented noncrystalline structure together with polymorphic structure consisting of predominantly Type I and a smaller proportion of Type III poly(*p*-oxybenzoate) structure. The resolved peak parameters in terms of *d*-spacings, half-height widths, and the corresponding apparent crystallite sizes are listed in Table VI. The apparent crystallite size evaluated for the peak at 0.454 nm as 8.8 nm corresponding to 19 laterally packed chains in the direction perpendicular to the (110) planes of Type I POB structure.

The curve fitting analysis reveals that 88% of the area above baseline is due to the oriented and ordered structure (see Table I). This means that the Vectran MK fiber consists of 12% unoriented noncrystalline structure. Taking into account the proportions of (110) and (220) reflections of Type I structure, a crystalline proportion of 24% is found.

Meridional analysis of Vectran MK fiber

Resolved meridional trace of Vectran MK fiber shown in Figure 13(a) can be resolved into three well-defined peaks with *d*-spacings of 0.664, 0.308, and 0.207 nm, respectively. The resolved peak parameters are listed in Table VI. The positions of the experimental meridional peaks listed in Table VI are shown to correspond to the predicted diffraction from isolated random copolymer chains using point²⁹ and atomic³⁰ modeling approaches for the 75/25 composition copolymer chains.

Using point and atomic modeling approaches, meridional scatter is shown to contain peaks with non-periodic character.^{29,30} The positions and relative intensities of meridional region were simulated using the atomic coordinates of random copolymer chain sequences taking into account the chemical rules. Chivers et al.³⁰ found good agreement between the simulated meridional intensity profiles and the experimental profiles using atomic modeling approach. The meridional peak at 0.21 nm was used to establish the persistence length of the extended chain conformation for various compositions. It appears that for the 75/25 composition, a persistence length of 13 units is required to give the peak width located at 0.21 nm.³⁰ Certainly, a similar length for the 73/27 composition

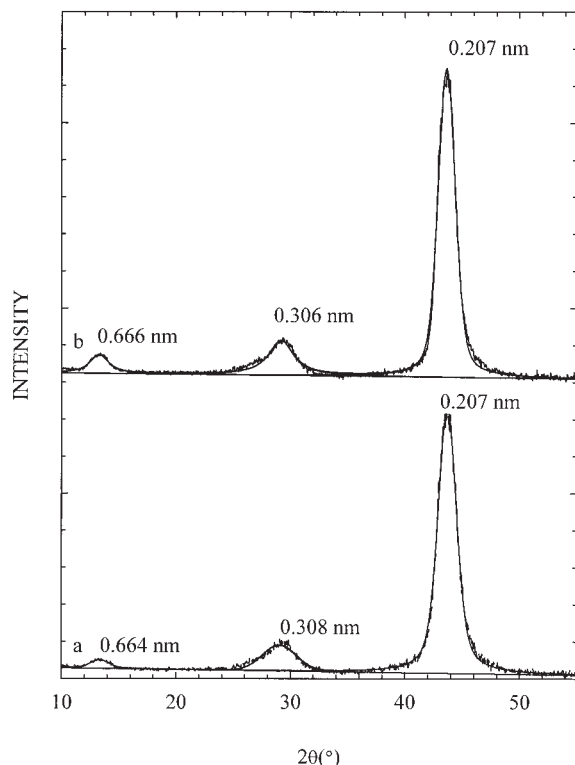


Figure 13 Curve fitting of meridional diffraction trace of (a) Vectran MK fiber and (b) Vectran HS fiber.

would be required to account for the meridional intensity profiles shown in Figure 13.

Meridional analysis of Vectran HS fiber

Resolved meridional trace of Vectran HS fiber shown in Figure 13(b) can be resolved into three well-defined peaks with d -spacings of 0.666, 0.306, and 0.207 nm, respectively. The resolved peak parameters are listed in Table VI. The corrected half-height width of Vectran HS fiber at 0.207 nm is 2.01° . The results suggest a slight change in the positions of the meridional peaks of Vectran HS fiber possibly due to the annealing process with slight narrowing of the peak widths, indicating longer persistence length of the copolymer chains.

Polarized infrared spectroscopy data analysis

Using the atomic modeling approach, Blackwell and coworkers^{30,31} showed that the simulated copolymer chains incorporating the trans conformations lead to a better agreement between the simulated and experimental meridional scatter in terms of interplanar d -spacings and intensity profiles. Therefore, the copolymer chains consisting of trans conformations will be assumed to be predominantly in the highly oriented and ordered (i.e., crystalline) structure. It will be fur-

ther assumed that the cis conformations to be predominantly in the unoriented and noncrystalline structure (i.e. totally amorphous phase). Of course the unoriented and noncrystalline (i.e. amorphous) phase is known to contain both trans and cis conformers.

As shown in Figures 10 and 11, HBA and HNA units are linked with each other through the ester groups forming predominantly trans conformations in the highly extended copolymer chains, whereas the homopolymers (Figs. 10(a) and 10(c)), poly(*p*-oxybenzoate), (i.e., HBA units in the copolymer chain) and poly(*p*-phenylene 2,6-naphthalate) (i.e., HNA units in the copolymer) are linked with each other forming cis conformations. The trans conformations in the crystalline phase lead to the highly extended chain conformations forming relatively good lateral packing organizations, whereas the cis conformations lead to the less extended and shorter chain conformations with poorer lateral packing organizations. In the models shown in Figure 11, the HBA and HNA units are shown to be parallel to the local chain axis making an angle of 0° with the local chain axis for the sake of simplicity. In the case of the copolymer chain models generated and used in the simulations by Blackwell and coworkers,^{30,31} the HBA and HNA units are found to make an average angle of $\pm 20^\circ$ with the local chain axis. This is the angle that will be used in the IR orientation calculations as the transition moment angle for the HBA and HNA units.

The IR spectrum of Vectran and poly(*p*-oxybenzoate) polymer (corresponding to HBA units in the Vectran fiber) in the $1670\text{--}1350\text{ cm}^{-1}$ region (shown in Figure 14) contains bands attributable to HBA and HNA units. Carbonyl (C=O) stretching vibration is located around $1730\text{--}1735\text{ cm}^{-1}$, showing perpendicular polarization characteristics but not shown in the spectrum. As can be seen in Figure 14(b), aromatic HBA ring vibrations are located at 1605 , 1510 , and 1415 cm^{-1} , showing relatively strong intensity values. In the IR spectrum of Vectran MK, shown in Figure 14(a), aromatic HBA bands are shifted to 1600 and 1507 cm^{-1} with no change in the position of 1415 cm^{-1} band. After discounting the aromatic HBA bands from the spectrum of Vectran, it becomes very obvious that the bands at 1632 and 1474 cm^{-1} correspond to the aromatic HNA units.

The IR band corresponding to HBA units located at 1600 cm^{-1} shows the highest dichroism (see Fig. 15(a)), whereas the IR band corresponding to HBA units located at 1415 cm^{-1} shows the lowest dichroism. Because of the nature of the highest dichroism, the 1600 cm^{-1} band is tentatively assigned to trans conformers in the crystalline phase, whereas the 1415 cm^{-1} band peak is assigned to the cis conformers in the unoriented noncrystalline phase. In the first instance, a transition moment angle of 20° is used as

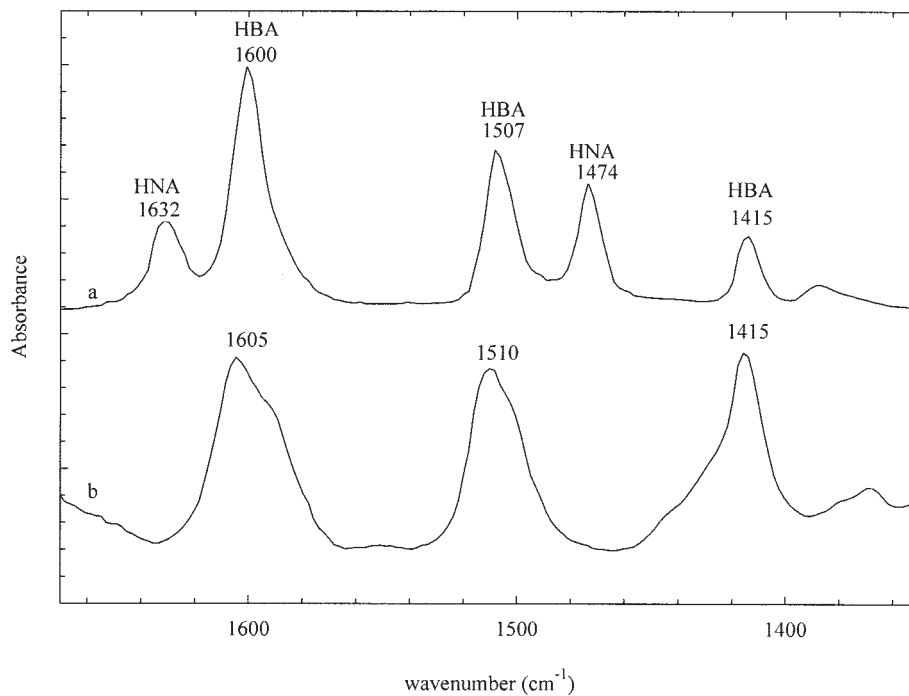


Figure 14 Infrared spectrum of (a) Vectran MK fiber and (b) poly(*p*-oxybenzoate) polymer.

suggested in the literature³⁰ for the HNA and HBA units. The corresponding $\langle P_2 \rangle$ values are listed in Table VII. When a transition moment angle of 22° for the C—C stretching vibrations in the HBA and HNA units of the copolymer chains is used,⁴⁹ the $\langle P_2 \rangle$ values are

found to be 3–4% higher when a transition moment angle of 20° is used. In effect, it appears that we do have a lower and upper limits for the transition moment angle for the HBA and HNA units. Indeed, Kaito et al.³² concludes in their IR study of the strands of

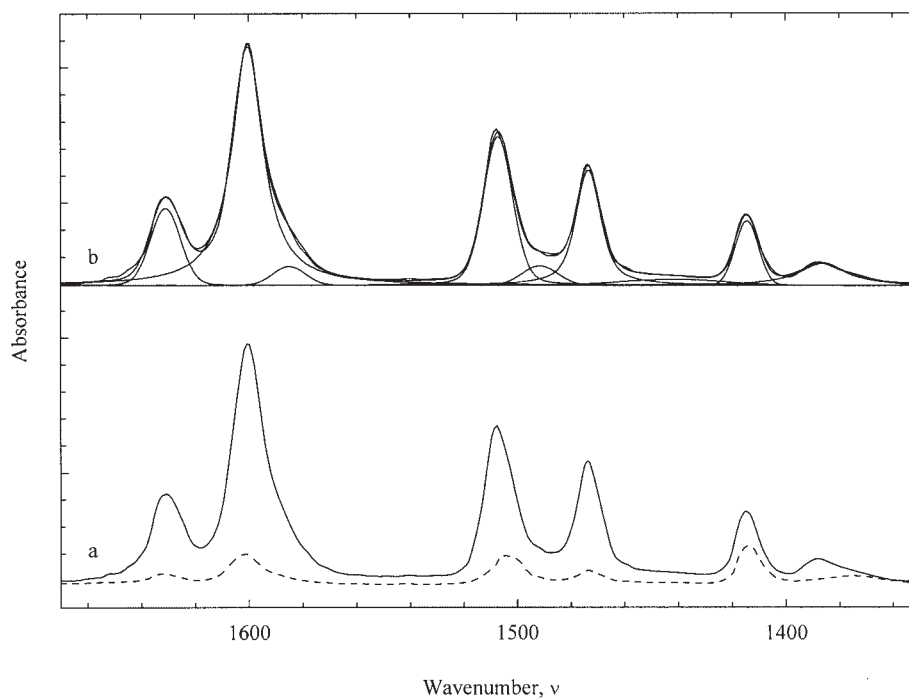


Figure 15 Polarised infrared spectra of Vectran MK fiber (a) continuous line is parallel spectrum, and broken line is perpendicular spectrum (b), an example of curve fitting.

TABLE VII
 $\langle P_2 \rangle$ Values of Vectran[®] Obtained from IR Data

Sample	HNA (1632 cm ⁻¹)	HBA (1600 cm ⁻¹)	HBA (1507 cm ⁻¹)	HNA (1474cm ⁻¹)	HBA (1415 cm ⁻¹)
Vectran [®] MK					
$\alpha = 20^\circ$	0.88 ± 0.04	0.84 ± 0.03	0.72 ± 0.03	0.87 ± 0.05	
$\beta = 22^\circ$	0.92 ± 0.04	0.88 ± 0.03	0.75 ± 0.03	0.91 ± 0.05	
$\alpha = 4^\circ$					0.20 ± 0.05
Vectran [®] HS					
$\alpha = 20^\circ$	0.94 ± 0.05	0.85 ± 0.04	0.75 ± 0.04	0.93 ± 0.04	
$\beta = 22^\circ$	0.98 ± 0.05	0.89 ± 0.04	0.78 ± 0.04	0.97 ± 0.04	
$\alpha = 4^\circ$					0.23 ± 0.04

HBA/HNA copolymer that the transition moment angle must be less than 24°.

In the case of the HBA units adopting the cis conformation in the homopolymer (poly(*p*-oxybenzoate; see Fig. 10(a)), the transition moment angle varies between 3.7° when the standard bond lengths and angles of Hummel and Flory⁵³ are used and 4.3° when the chain conformation of Liu et al.⁵⁴ is considered. Since the transition moment angles of 3.7° and 4.3° are very close to each other, the net effect on the calculated $\langle P_2 \rangle$ values will be very small indeed. In our case, we have taken an average angle of 4° as the transition moment angle of the HBA units forming cis conformations in the unoriented noncrystalline phase.

As shown in Figure 15(b), curve fitting is carried out to obtain integrated absorbance values based on a combination of Gaussian and Lorentzian profiles. During the curve fitting procedures, it was necessary to include peaks at 1585, 1491.7, and 1441.7 cm⁻¹ to improve the fitting but these peaks are not used in the calculations. The calculated $\langle P_2 \rangle$ values corresponding to the HBA and HNA units of Vectran MK and Vectran HS fibers are listed in Table VII. The $\langle P_2 \rangle$ values of the HBA unit of Vectran MK fiber arising from 1600 and 1507 cm⁻¹ trans bands are found to vary between 0.84–0.88 ± 0.04 and 0.72–0.75 ± 0.04 depending on which transition moment angle is used. The $\langle P_2 \rangle$ value of 0.2 ± 0.05 is obtained from the 1415 cm⁻¹ cis band, whereas the $\langle P_2 \rangle$ value of the HNA unit of Vectran MK fiber arising from the 1632 and 1475 cm⁻¹ trans bands are found to vary between 0.88–0.92 ± 0.04 and 0.87–0.91 ± 0.05, respectively. It clearly shows that HNA units are slightly more oriented than the HBA units of the copolymer chains in the oriented and ordered phase. A similar relationship exists between the $\langle P_2 \rangle$ values of the HBA and HNA units of Vectran HS fiber. As shown in Table VII, the $\langle P_2 \rangle$ values of Vectran HS fiber are on average 6% higher for the HNA units and 1–3% higher for the HBA units than that of Vectran MK fiber.

The total trans conformer content of Vectran MK and Vectran HS fibers in the ordered (i.e., crystalline) phase is obtained using eqs. (7) and (8) as the sum of

the integrated absorbance values of IR bands at 1632, 1600, 1508, and 1475 cm⁻¹ assigned to trans conformers in the ordered phase. The IR band at 1415 cm⁻¹ is assigned to cis conformer in the unoriented and noncrystalline phase (i.e. totally amorphous phase). The results show a total trans and cis conformer content of (85 ± 1)% and (15 ± 1)%, respectively, for the Vectran MK fiber. As shown in Table VIII, the trans conformer contents of HBA and HNA units in the oriented and ordered phase are obtained using 1600 and 1508 cm⁻¹ HBA unit vibrations and 1632 and 1415 cm⁻¹ HNA unit vibrations for the Vectran MK fiber as (57 ± 1)% and (28 ± 1)%, respectively.

As shown in Table VIII, the total trans conformer content in the oriented and ordered phase and cis conformer content in the unoriented and noncrystalline phase of Vectran HS fiber are on average 3% higher in the case of total trans conformer content and 3% lower in the case of total cis conformer content than that of Vectran MK fiber.

Mechanical properties

The measured mechanical properties of Vectran MK fiber are listed in Table IX. The results suggest a tensile strength of 1.27–1.37 GPa, an elongation at break of 1.9–2.2%, and a tensile modulus of 60.5–78.9 GPa for the Vectran MK fiber depending on the testing conditions. In the case of the Vectran HS fiber, as shown in Table IX, a tensile strength of 2.89–3.02 GPa, an elongation at break of 3–3.4%, and a tensile modulus of 64–85.9 GPa depending on the testing conditions are obtained.

TABLE VIII
 Total Trans and Cis Conformer Contents of Vectran[®] Fibers

Sample	Total χ_{trans} (%)	HBA χ_{trans} (%)	HNA χ_{trans} (%)	Total χ_{cis} (%)
Vectran [®] MK	85	57	28	15
Vectran [®] HS	88	64	24	12

TABLE IX
Tensile Testing Results

Cross head speed (mm/min)	Tensile strength (GPa)	Extension at break (%)	Tensile modulus (GPa)
PET-FOY			
160	1.06 ± 0.5	11.4 ± 1.3	9.7 ± 0.3
200	1.06 ± 0.4	11.0 ± 4.1	10.3 ± 4.2
500	0.90 ± 0.4	9.4 ± 4.2	12.3 ± 4.2
PEN-FOY			
160	0.98 ± 0.4	11.0 ± 0.9	19.9 ± 0.6
200	0.96 ± 0.1	10.9 ± 0.6	20.1 ± 0.4
500	0.89 ± 0.1	9.4 ± 1.0	20.6 ± 0.6
Vectran [®] MK			
160	1.37 ± 0.04	2.2 ± 0.05	60.5 ± 1.88
200	1.34 ± 0.04	2.1 ± 0.08	64.7 ± 1.25
500	1.27 ± 0.03	1.9 ± 0.05	78.9 ± 1.5
Vectran [®] HS			
160	3.02 ± 0.14	3.4 ± 0.11	64.0 ± 2.1
200	2.99 ± 0.16	3.3 ± 0.08	68.7 ± 2.5
500	2.89 ± 0.13	3.0 ± 0.08	85.9 ± 1.9

The results listed in Table IX show that Vectran HS fiber appears to have significantly enhanced tensile strength and modulus than that of Vectran MK fiber. Usually the increase in tensile strength is known to be due to the increases in the molecular weight increase, whereas the increase in tensile modulus is usually attributed to the increase in the molecular orientation. The X-ray modulus for the HBA/HNA tapes (20 μ m thick and 5 mm wide) consisting of 73% HBA units and 27% HNA units at room temperature by recording the shift of the interplanar *d*-spacing of 0.21 nm as a function of applied stress in the axial direction is reported⁵⁰ to be 105 GPa. Normally, the X-ray modulus measurements give the theoretical upper limit for the oriented and ordered phase. If we consider the X-ray modulus values as the theoretical upper limit, then, the tensile modulus of Vectran MK and Vectran HS fibers correspond to 75 and 82% of the theoretical upper limit of tensile modulus measurements carried out at room temperature.

It is clear that there is still some room for improvement for the tensile modulus of Vectran fibers. Of course longer annealing times may enhance the tensile properties at an additional cost of annealing treatments.

CONCLUSIONS

A comparative study of structure and properties of commercially available thermoplastic and thermotropic polyester fibers have been carried out using optical birefringence, infrared spectroscopy, wide-angle X-ray diffraction, and tensile testing methods. The

results show the enhancement of birefringence and tensile modulus values arising from the replacement of *p*-phenylene ring in PET with stiffer and bulkier naphthalene ring in PEN structure. In the case of the thermotropic polyesters, fully extended chain sequences consisting of aromatic moieties contained in the backbone structure lead to highly oriented and highly ordered lateral structure together with enhanced tensile properties.

Infrared spectroscopy has been utilized in the determination of crystallinity values through the evaluation of trans conformer contents in the crystalline phase. The results obtained from polarized infrared spectroscopy data of highly oriented PET and PEN fibers show that trans conformers in the crystalline phase are more highly oriented than gauche conformers in the amorphous phase. Analysis of X-ray diffraction traces and infrared spectra shows the presence of polymorphic structure consisting of α - and β -phase structures in the fully oriented PEN fiber. The results suggest that the trans conformers in the β -phase is more highly oriented than the α -phase.

Equatorial X-ray diffraction analysis of Vectran MK fiber suggests a lateral organization arising from high temperature modification of poly(*p*-oxybenzoate) structure with a degree of crystallinity of 22%. In the case of the Vectran HS fiber, the lateral structure is shown to contain regions adopting lateral chain packing similar to the room temperature modification of Type I structure of poly(*p*-oxybenzoate) with a degree of crystallinity of 24%. Both fibers are shown to possess predominantly oriented noncrystalline structure together with a smaller proportion of oriented crystalline and unoriented noncrystalline materials.

The author thanks Celanese Acetate LLC of USA for the Vectran[®] yarns and Teijin Ltd of Japan for the fully oriented PET and PEN yarns investigated in the present study. Thanks also go to G. Azmi Kocaker, Bulent Dal, and Alison Edmed for the assistance during the experimental work. Ian Brough of Materials Science Centre of UMIST (UK) is very much appreciated for his assistance with the X-ray diffraction work. Special thanks go to an anonymous reviewer for making useful comments.

References

1. Anonim, Melliand Int 2004, 10, 148.
2. Wilson, D. K.; Kollu, T. Text Prog 1987, 16, 1.
3. Daubeny, R.; de, P.; Bunn, C. W.; Brown, C. J. Proc R Soc London Ser A 1954, 226, 531.
4. Yazdaniyan, M.; Ward, I. M.; Brody, H. Polymer 1985, 26, 1779.
5. Wu, G.; Tucker, P. A.; Cuculo, J. A. Polymer 1997, 38, 1091.
6. Sharma, V.; Desai, P.; Abhiraman, A. S. J Appl Polym Sci 1997, 65, 2603.
7. Donnelly, A.; Ohara, T.; Birkinshaw, C. J Appl Polym Sci 1997, 66, 989.
8. Lim, J. Y.; Kim, S. Y. J Appl Polym Sci 1999, 71, 943.
9. Suzuki, A.; Okano, T. J Appl Polym Sci 2004, 92, 2989.

10. Jarvis, D. A.; Hutchinson, I. J.; Bower, D. I.; Ward, I. M. *Polymer* 1980, 21, 41.
11. Chen, W.; Lofgren, E. A.; Jabarin, S. A. *J Appl Polym Sci* 1998, 70, 1965.
12. Middleton, A. C.; Duckett, R. A.; Ward, I. M.; Mahendrasingham, A.; Martin, C. *J Appl Polym Sci* 2001, 79, 1825.
13. Overall, N.; MacKerron, D.; Winter, D. *Polymer* 2002, 43, 4217.
14. Zhang, Y.; Lu, Y.; Duan, Y.; Zhang, J.; Yan, S.; Shen, D. *J Polym Sci Part B: Polym Phys* 2004, 42, 4440.
15. Zhang, Y.; Lu, Y.; Yan, S.; Shen, D. *Polymer J* 2005, 37, 133.
16. Marco, Y.; Chevalier, L.; Chaouche, M. *Polymer* 2002, 43, 6569.
17. Carr, P. L.; Zhang, H.; Ward, I. M. *Polym Adv Technol* 1996, 7, 39.
18. Miyata, K.; Kikutani, T.; Okui, N. *J Appl Polym Sci* 1997, 65, 1415.
19. Cakmak, M.; Kim, J. C. *J Appl Polym Sci* 1997, 64, 729.
20. van den Heuvel, C. J. M.; Klop, E. A. *Polymer* 2000, 41, 4249.
21. Wu, G.; Liu, M.; Li, X.; Cuculo, J. A. *J Polym Sci Part B: Polym Phys* 2000, 38, 1424.
22. Suzuki, A.; Koide, C. *J Polym Sci Part B: Polym Phys* 2000, 38, 61.
23. Chae, H. G.; Chae, D. W.; Kim, B. C.; Seo, S. W. *J Appl Polym Sci* 2002, 83, 916.
24. Hardy, L.; Stevenson, I.; Voice, A. M.; Ward, I. M. *Polymer* 2002, 43, 6013.
25. Wu, G.; Cuculo, J. A. *Polymer* 1999, 40, 1011.
26. Flory, P. J. *Proc R Soc London Ser A* 1954, 243, 73.
27. Dobb, M. G.; McIntyre, J. E. *Adv Polym Sci* 1984, 60/61, 61.
28. Cox, M. K. *Mol Cryst Liq Cryst* 1987, 153A, 415.
29. Gutierrez, G. A.; Chivers, R. A.; Blackwell, J.; Stamatoff, J. B.; Yoon, H. *Polymer* 1983, 24, 937.
30. Chivers, R. A.; Blackwell, J.; Gutierrez, G. A.; Stamatoff, J. B.; Yoon, H. *Polymer* 1984, 25, 435.
31. Chivers, R. A.; Blackwell, J. *Polymer* 1985, 26, 997.
32. Kaito, A.; Kyotani, M.; Nakayama, K. *Macromolecules* 1991, 24, 3244.
33. Taylor, J. E.; Romo-Urbe, A.; Libera, M. R. *Polym Adv Technol* 2003, 14, 595.
34. Hindeleh, A. M.; Johnson, D. J.; Montague, P. E. In *Fiber Diffraction Methods*; French, A. D., Gardner, K. H., Eds.; ACS Symp Ser 141; American Chemical Society: Washington, DC, 1983; p 149.
35. Stokes, A. R. *Proc Phys Soc London Sect A* 1948, 166, 283.
36. Karacan, I.; Bower, D. I.; Ward, I. M. *Polymer* 1994, 35, 3411.
37. Hindeleh, A. M.; Johnson, D. J. *Polymer* 1978, 19, 27.
38. Mencik, Z. *Chem Prumsyl* 1967, 17, 78.
39. Buchner, S.; Wiswe, D.; Zachman, H. G. *Polymer* 1989, 30, 480.
40. Cunningham, A.; Ward, I. M.; Willis, H. A.; Zichy, V. *Polymer* 1974, 15, 749.
41. Ouchi, I.; Hosoi, M.; Shimotsuna, S. *J Appl Polym Sci* 1977, 21, 3445.
42. Nakamae, K.; Nishino, T.; Gotoh, Y. *Polymer* 1995, 36, 1401.
43. Bang, Y. H.; Lee, S. H.; Kwon, I. H.; Cho, H. H. *J Appl Polym Sci* 2004, 94, 1265.
44. Blackwell, J.; Lieser, G.; Gutierrez, G. A. *Macromolecules* 1983, 16, 1418.
45. Sun, Z.; Cheng, H.-M.; Blackwell, J. *Macromolecules* 1991, V24, 4162.
46. Salahshoor-Kordestani, S.; Hanna, S.; Windle, A. H. *Polymer* 2000, 41, 6619.
47. Blundell, D. J. *Polymer* 1982, 23, 359.
48. Plummer, C. J. G.; Kausch, H.-H. *Polymer* 1987, 38, 1745.
49. Wiberg, G.; Gedde, U. W. *Polymer* 1997, 38, 3753.
50. Green, D. I.; Unwin, A. P.; Davies, G. R.; Ward, I. M. *Polymer* 1990, 31, 579.
51. Lieser, G. *J Polym Sci Polym Phys Ed* 1983, 21, 1611.
52. Coulter, P. D.; Hanna, S.; Windle, A. H. *Liq Cryst* 1989, 5, 1603.
53. Hummel, J. P.; Flory, P. J. *Macromolecules* 1980, 13, 479.
54. Liu, J.; Yuan, B.-L.; Geil, P. H.; Dorset, D. L. *Polymer* 1997, 38, 6031.